CHEMISTRY OF MATERIALS
Cite This: Chem. Mater. 2019, 31, 9307−9316
Article
pubs.acs.org/cm

Extending the Spectral Range of Double-Heterojunction Nanorods by Cation Exchange-Induced Alloying

Joseph C. Flanagan, Logan P. Keating, Muttanagoud N. Kalasad,† and Moonsub Shim*

Department of Materials Science and Engineering and Frederick Seitz Materials Research Laboratory, University of Illinois at Urbana-Champaign, Urbana, Illinois 61801, United States

Supporting Information

ABSTRACT: Composition variation and formation of core/shell heterostructures have allowed the extension and applicability of size-tunable optical properties of colloidal semiconductor nanocrystals. Anisotropic shapes such as nanorods (NRs) provide new and further refined properties but relatively simple and empowering approaches such as alloying and controlled heterostructure formation are much more challenging to apply to these materials. Here, we start from a well-defined CdS/CdSe barbell-shaped NR heterostructure and perform sequential cation exchanges first with Cu and then with Cd/Zn under relatively mild conditions to achieve alloying while preserving the structure. By using a mixture of Cd and Zn in the presence of a thiol, controllable amounts of alloying in both components could be achieved. Growth of a final ZnSe shell enhances the photoluminescence and allows the creation of a series of double-heterojunction NRs with emission spanning the visible spectral range.

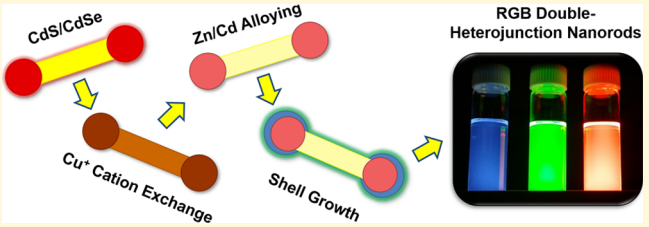

INTRODUCTION

Colloidal semiconductor nanocrystals (NCs) are a growing class of materials gaining wide applicability because of their tunable shape and band gap. Heterojunctions of two or more materials can be synthesized to tailor their properties further. Type-I straddling band offset core/shell structures are the most common example, with a larger band gap shell confining charge carriers to the core, thereby enhancing the photoluminescence (PL) and making them particularly suitable for bioimaging, lighting, displays, and luminescent solar concentrators.[1−4] Type-II staggered band offset heterojunctions that separate charges can be beneficial for photovoltaics and catalysis.[5−9] Introduction of additional functional heterointerfaces, as in double-heterojunction nanorods (DHNRs) with p−i−n-like band alignment,[10] has led to the enhancement in NC-based light-emitting diodes (LEDs)[11] and has added bidirectionality of light emission and detection to these LEDs.[12] These capabilities result from the anisotropic shape along with the band alignment of the CdS, CdSe, and ZnSe components, as summarized in Scheme 1. CdS and ZnSe both make type-I junctions with CdSe to enhance PL, but CdS and ZnSe form a type-II junction with each other. This well-known double heterostructure, combined with the anisotropic shape of the rod, facilitates electron and hole injection/blocking and provides accessibility and directionality for both types of carriers. However, DHNRs are currently spectrally limited to orange/red emission from the CdSe band edge. This limitation arises mainly from etching and ripening of the CdS/CdSe heterojunction nanorods (HNRs) during the ZnSe growth step.[13] That is, even if the starting CdSe/CdS/CdSe rod/rod/rod HNRs emitted in the green, oleate-induced etching of CdS and CdSe and the presence of Se precursors causes CdSe tips to ripen, converting CdS/CdSe HNRs into barbell shapes prior to ZnSe shell growth and red-shifting the PL peak position. Hence, an alternative to size control appears necessary in extending the spectral range of emission of DHNRs.

One potential approach may be alloying with Zn. Furthermore, because of the large band gap of ZnSe, $Cd_xZn_{1-x}Se$ alloys should be able to emit across the entire visible spectrum including blue emission which is difficult to

Scheme 1. Energy Band Diagram for DHNRs[10a]

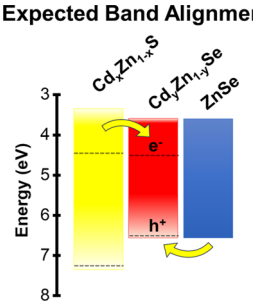

[a]The dotted lines indicate the conduction and valence band positions of pure CdS and CdSe. Alloying can extend the accessible range of band edges all the way to pure ZnS and ZnSe. At any given intermediate composition, the appropriate hole and electron-injecting band offsets should be preserved.

Received: July 2, 2019
Revised: October 28, 2019
Published: October 31, 2019

DOI: 10.1021/acs.chemmater.9b02615
Chem. Mater. 2019, 31, 9307−9316

achieve with pure CdSe by size control alone. By alloying the CdS rod in tandem, the proper conduction band alignment can be maintained. However, direct growth of alloyed $Cd_xZn_{1-x}S$ nanorods (NRs) is not straightforward. Typically, small-diameter Zn chalcogenide nanowires are grown first and then transformed to NRs through a high-temperature ripening process.[14,15] ZnS and ZnSe NCs can be alloyed with Cd through cation exchange by annealing them in the presence of Cd-oleate (Cd-OA),[16] but the alloying is nonuniform if the temperature is too low,[17] and a loss of size distribution and/or shape can occur when anisotropic rods are used at higher temperatures.[18] On the other hand, CdS and CdSe NCs cannot be directly alloyed with Zn through cation exchange due to the similar chemical hardness of the metal ions but higher stability of Cd-chalcogenides and therefore must proceed through an intermediate Cu exchange step to be converted to Cd_xZn_{1-x} chalcogenide NCs.[19−21] $Cu_{2-x}S$ has received significant attention recently as a template for the synthesis of alloys and complex heterostructures via cation exchange,[22−24] which has the advantage of preserving the anion sublattice and therefore overall shape of NCs, but direct Cd/Zn alloying from Cu-based NCs has not been demonstrated to our knowledge. A recent report by Yuan et al. demonstrates Cu-mediated alloying of core/shell heterostructures, but the method requires the simultaneous growth of a $Cd_xZn_{1-x}S$ shell, and the high reaction temperature may render the method unfeasible for most other anisotropic structures.[25] Direct synthesis by decomposing single-source metal-diethyldithiocarbamate has also been demonstrated,[26−28] but it is difficult to control the size distribution, especially with increasing Cd content, and it is unlikely that uniform heterostructures with Se could be synthesized through the same method.

Here, we detail a general approach to achieve anisotropic Cd_xZn_{1-x} chalcogenide heterostructures where a Cd-based structure with a well-established synthesis undergoes sequential cation exchange reactions to achieve the desired alloy composition (Scheme 2). As a proof-of-concept, we focus on converting CdS/CdSe HNRs through cation exchange with Cu and then with mixtures of Cd and Zn, demonstrating band gap tunability while maintaining delicate structural features. Selective growth of ZnSe on the resulting alloyed HNRs leads to DHNRs with emission that can span the entire visible spectral range.

Scheme 2. Process Flow for Creating Alloyed DHNRs[a]

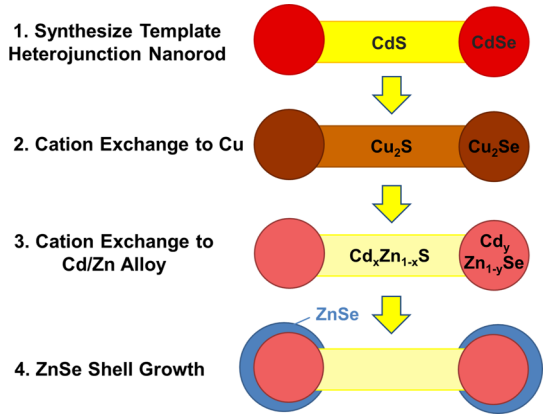

[a]Following the synthesis of CdS/CdSe HNRs, sequential Cu and Cd/Zn cation exchange reactions are carried out to achieve the desired alloy composition. Finally, a ZnSe shell is grown to improve the PL.

RESULTS AND DISCUSSION

There are several challenges, beyond those that have been addressed in "spherical" NCs, in achieving heterostructures of semiconductor NRs through multistep cation exchange. First, whether induced during the cation exchange reaction or the intermediate purification step, NRs are more prone to aggregation due to their larger typical size. Aggregation/precipitation from the reaction mixture can hinder the cation exchange reaction and lead to undesired coalescence. Second, milder reaction conditions may be necessary to avoid effects such as ripening to maintain the rod shape and the spatial distribution of the composition. Furthermore, achieving desired alloy composition requires control over exchange rates of different target cations, which may be significantly different for available combinations of solvents, ligands, and precursors. The barbell structure of CdS and CdSe explored here represents one of the simplest and the best-established materials beyond the core/shells that introduce structural anisotropy and epitaxial heterointerfaces. They also form the basis of DHNRs. Details of the synthesis are available in the Supporting Information. Below, we discuss the salient aspects of the challenges in each step of our cation exchange approach to alloyed HNRs and how we addressed these issues.

Cd-to-Cu Cation Exchange. Given recent advances in the conversion of several different types of Cd-based NCs, including CdSe/CdS dot-in-rod structures, to Zn-based counterparts through cation exchange, our initial efforts followed established literature procedures.[20,29] These CdS/CdSe HNRs were first examined using tetrakis(acetonitrile)-copper(I) hexafluorophosphate ($[Cu(CH_3CN)_4]PF_6$) and methanol to exchange Cd to Cu, followed by $ZnCl_2$ and trioctylphosphine (TOP) to achieve ZnS/ZnSe HNRs. While we were able to achieve complete Cu and Zn cation exchange, we encountered a problem with NR aggregation during the Cu exchange step. Starting from single-composition CdS and CdSe NRs, respectively, Sadtler et al. have mentioned branched structures being formed during Cu cation exchange,[29] and Li et al. have noted that repeated washing causes massive aggregation after Cu exchange.[19] However, neither report has explored this issue in depth. We examined both CdS/CdSe HNRs and their CdS-only seeds as a control experiment, and our results show extensive tip-to-tip coalescence of NRs in both cases, especially after Cu exchange (Supporting Information, Figure S1a).

The observed aggregation is most likely a result of ligand loss; therefore the addition of excess free ligands to the reaction mixture was considered and examined. Kriegel et al. have used oleylamine to compensate for the ligand loss[30] but Sadtler et al. have noted that excess octylamine prevents complete cation exchange, possibly due to binding with free Cu^+.[29] We found that in the presence of oleylamine, an intermediate structure consisting of Cd-rich rods with a second phase nucleated on them [observed as a dark circular spot on each rod in transmission electron microscopy (TEM)], even when an excess amount of Cu ions (up to 12 Cu^+ to 1 Cd^{2+}) are present in the reaction mixture (Supporting Information, Figures S1b,c). When this intermediate was exchanged with Zn^{2+}, the optical properties resemble the starting CdS/CdSe HNRs but with a smaller average size, indicating that the

DOI: 10.1021/acs.chemmater.9b02615
Chem. Mater. 2019, 31, 9307−9316

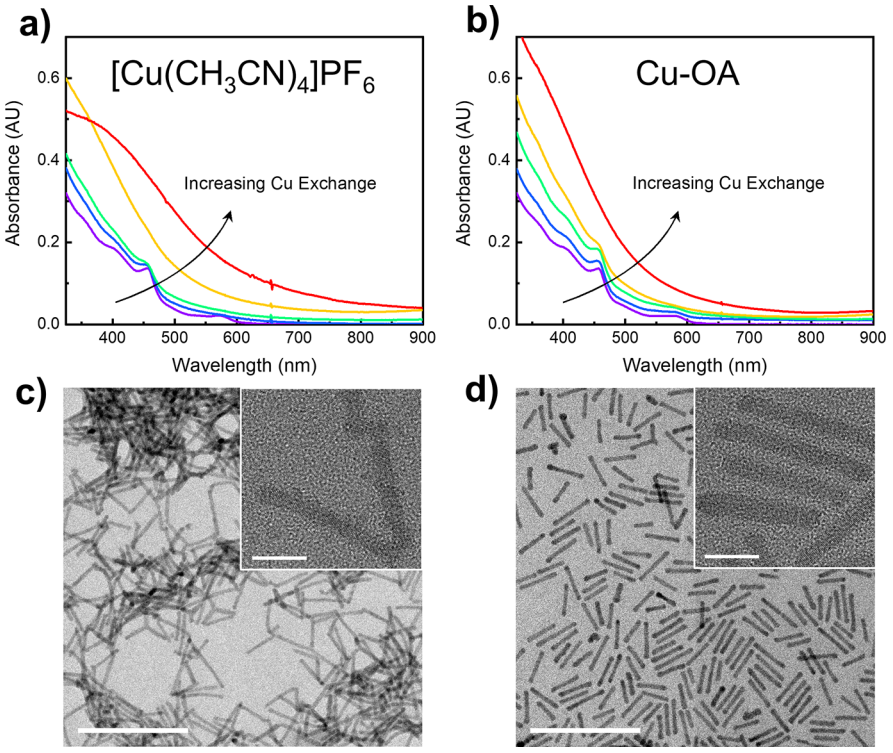

Figure 1. Absorption spectra of CdS/CdSe HNRs as (a) $[Cu(CH_3CN)_4]PF_6$ in methanol or (b) Cu-OA solution is added incrementally. In the order of increasing optical density, 0, 10, 20, 50, and 100 μmol Cu(I) ion was added. The final sample in (a) had aggregated leading to the scattering observed in the absorption spectrum. (c) Low-resolution TEM image of a loose network of aggregated Cu-HNRs from cation exchange using $[Cu(CH_3CN)_4]PF_6$. The inset is a high-resolution image, showing rods joined at the tips. (d) Low and high-resolution TEM images showing well-dispersed HNRs after Cu exchange employing Cu-OA. The scale bars represent 100 nm for the low-resolution and 10 nm for the high-resolution images.

cation exchange was incomplete (Supporting Information, Figure S2). Therefore, we looked for alternative ligands.

First, using one of the most common ligands, trioctylphosphine oxide (TOPO), the severity of aggregation could be reduced compared to a reaction without excess ligands. However, it could not be eliminated completely. While exploring metal-oleates as stabilizers, we found that Cu(I)-oleate (Cu-OA) can be used to initiate cation exchange at room temperature without the addition of methanol, which is typically employed as a hard base to solvate Cd^{2+} ions[21] and which we suspect contributes to NR aggregation. The details of Cu-OA precursor preparation, example photographs, and the absorption spectra of Cu-OA are included in the Supporting Information (Figure S3). When Cu-OA was added to the CdS/CdSe HNR solution, cation exchange occurred, but the resulting HNRs still aggregated. However, if free oleylamine was added to the HNR solution first, the HNRs remained well-dispersed while still undergoing complete cation exchange.

Figure 1 compares Cu cation exchange reactions using $[Cu(CH_3CN)_4]PF_6$ with TOPO as a stabilizer and Cu-OA with oleylamine as a stabilizer. The progress of the Cu cation exchange reaction can be tracked by measuring the UV/vis absorption spectra (Figure 1a,b). As more Cu is added, the absorption peak/shoulder corresponding to CdS and CdSe band edge transitions become less distinct, but the overall optical density increases, as expected for the formation of the $Cu_{2-x}X$ compounds.[19] Increase of the optical density at 800 nm and beyond (i.e., nonzero baseline) is attributed to the localized surface plasmon resonance (infrared absorbance shown in Figure S4) due to off-stoichiometry doping commonly observed in Cu-based NCs,[31] whose position depends on the degree of oxidation.[32] To determine how much Cu was needed for complete exchange, the Cu source was added incrementally and 100 μL aliquots were taken from the reaction mixture after each addition. The Cu exchange was deemed complete once the measured optical density at 400 nm began to decrease, indicating that the added solution was merely causing a dilution of the reaction mixture. Note that Cu-OA in oleylamine exhibits very little absorption at this wavelength (Figure S3c). An example of aggregates arising from cation exchange using $[Cu(CH_3CN)_4]PF_6$ with TOPO is shown in Figure 1c. The rods appear to fuse predominantly at the tips, displaying continuous lattice fringes, and cannot be completely redispersed by sonication. However, when Cu-OA and oleylamine are used, scattering is not observed and the HNRs stay well-dispersed (Figure 1b,d). The use of $[Cu(CH_3CN)_4]PF_6$ is ubiquitous in the literature, but the reaction conditions needed lead to a severe problem of aggregation for NRs. Aggregated HNRs also display weak band edge PL after Zn/Cd exchange (Supporting Information Figure S5). When severely aggregated, PL is not observed over the scattering background. Therefore, solving the aggregation problem is critical to realizing high-performance DHNRs. In addition to reducing aggregation, using Cu-OA as the Cu source has other advantages. First, it can be synthesized easily from common and low-cost reagents, Cu acetate and oleic acid. Second, it enables the cation exchange reaction to be performed entirely in nonpolar solvents, preventing unwanted flocculation before the completion of the reaction.

DOI: 10.1021/acs.chemmater.9b02615
Chem. Mater. 2019, 31, 9307−9316

Cu-to-Cd/Zn Cation Exchange. For the second cation exchange step, a solution of $ZnCl_2$ and oleylamine served as the Zn^{2+} source/precursor with TOP as the base to extract Cu(I). To achieve alloys of cations Zn and Cd, the amounts of $CdCl_2$ and $ZnCl_2$ were systematically varied. Because of the higher reactivity of the Cd compound over Zn for the cation exchange reaction,[19] addition of an excess amount of Zn was first attempted. Furthermore, better Cu extraction and higher PL quantum yield (QY) of the final product has been reported at temperatures above 200 °C, while shape change can occur at temperatures above 250 °C.[20] Hence, cation exchange with an excess amount of Zn (1:20 ratio of Cd to Zn) was carried out at 220 °C. Only a broad emission at short times, ripening of the tips on some of the rods, and the appearance of emission near the CdSe band edge at longer times were observed (Supporting Information, Figures S6a,b). At high temperatures, $CdCl_2$ appears to be too reactive and incorporates much faster than Zn. Given that complete Cd cation exchange has been reported even at room temperature,[33] we next chose an intermediate temperature of 150 °C with a 1:10 ratio of Cd to Zn. We still observed undesirable results (Supporting Information, Figure S6c,d). While this temperature appears to be low enough to prevent shape change/ripening, Cd incorporation is still far more favorable, as indicated by the resulting emission being near the CdSe band edge. In addition, the alloying appears nonuniform, as suggested by the double-peaked emission from a sample which initially had HNRs with only a single emission peak.

As temperature and Cd/Zn ratio alone appeared to be insufficient to control the degree of Cd incorporation, addition of ligands to suppress the reactivity of the Cd precursor was then considered. Cd−thiol complexes have been shown to be more stable than Zn−thiol complexes but less than Cu(I)−thiol complexes.[34,35] According to Pearson's hard-soft acid−base theory, the softer Cd^{2+} ion should coordinate more favorably with the thiol, a soft base, than Zn^{2+}.[21,36] Therefore, the addition of thiols to the reaction mixture may reduce Cd reactivity without interfering with Cu(I) extraction. Under our optimized conditions, 0.5 mL of 1-octanethiol was added to the TOP solution containing $Cu_{2-x}S/Cu_{2-y}Se$ HNRs and then injected into a solution containing 1 mmol $ZnCl_2$ and varying amounts of $CdCl_2$ at 150 °C. Figure 2 shows X-ray diffraction (XRD) and TEM images of starting CdS/CdSe and HNRs exchanged with 1:4, 1:25, and 0:1 ratios of Cd to Zn added to the reaction mixture. The XRD results (Figure 2a) show a good match to the wurtzite crystal structure. In particular, a sharp peak corresponding to the (002) plane is observed in all samples, which matches reasonably well with the expected positions of pure ZnS and CdS. A strong (002) peak is observed due to the "texture" of the sample. HNRs grow along the [001] direction, and when drop-cast onto a substrate, they tend to lie flat, favoring diffraction from the (002) plane. Although the HNRs contain both selenide and sulfide components, the volume of the sulfide component is much higher and dominates the XRD signal. However, some shift from the expected structure arises due to the presence of the selenide component and interfacial strain. The position of the (002) peak can be observed at intermediate values for the alloyed samples. TEM images show that the rod structure is maintained throughout the cation exchange reactions and the resulting HNRs are not irreversibly aggregated. Further TEM images of the HNRs before and after cation exchange for

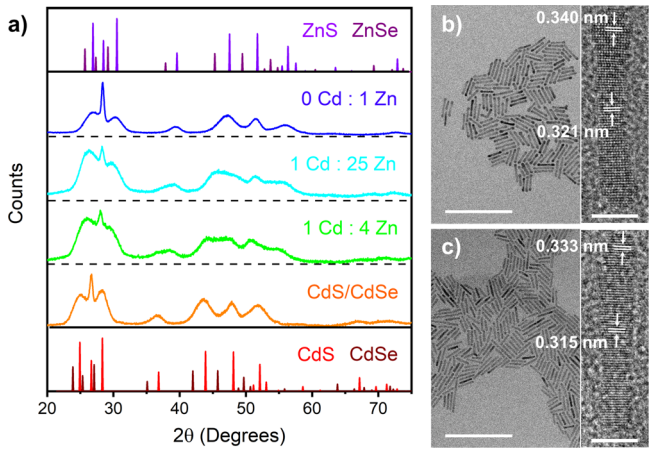

Figure 2. (a) XRD results for starting CdS/CdSe HNRs and HNRs that have undergone Cu and then Cd/Zn cation exchange with reagents having Cd/Zn ratios of 1:4, 1:25, and 0:1. Simulated patterns for wurtzite ZnS (PDF#97-006-7453) and CdS (PDF#97-006-7776) are provided for comparison. Simulated ZnSe (PDF#97-065-2217) and CdSe (PDF#97-060-0366) patterns are provided as well at half intensity and darker shade. Low-resolution TEM images of 1:4 (b) and 1:25 (c) Cd/Zn ratio samples, with high-resolution images of a single rod as the insets. The scale bars correspond to 100 and 5 nm for low- and high-resolution images, respectively.

different Cd/Zn ratios are included in the Supporting Information (Figure S7).

In order to better characterize the structure and composition of the resulting alloyed HNRs, particularly the elemental distribution, high angle annular dark field (HAADF), scanning TEM (STEM), and energy-dispersive X-ray spectroscopy (EDS) mapping were carried out. An example HAADF image of HNRs exchanged with a 1:4 Cd/Zn ratio solution is shown in Figure 3a. By Vegard's Law, the observed lattice spacings correspond to compositions of 36% Cd in the center of the rods and 55% Cd at the tips. The HAADF intensity is also greater at the tips, but this is expected due to the presence of Se and the slightly larger diameter. No other obvious bright spots are visible, which means that there are likely no separate pure CdS regions in the center of the rods due to nonuniform alloying.

EDS maps of the HNRs were collected to more accurately determine the elemental distribution and are shown in Figure 3b (Supporting Information Figure S8 for HNRs from 1:25 Cd/Zn ratio solution). By plotting only S and Se distributions, we can clearly see that the Se is present only at the tips, which is expected as the anion sublattice should remain intact during cation exchange. Both Cd and Zn are present throughout the length of the rods, but Cd does appear to be more concentrated at the tips. We integrated the tips and centers of the rods separately to quantify the Cd and Zn concentrations of each compound. EDS measurements confirm that the centers of the rods have slightly lower Cd concentration than the tips, with the measured composition being $Cd_{0.35}Zn_{0.65}S/Cd_{0.52}Zn_{0.48}Se$ for the sample shown in Figure 3.

The UV/vis absorption and PL spectra of HNRs of varying degree of alloying are shown in Figure 4. At complete Zn exchange, both ZnS and ZnSe band edge shoulders can be seen in the absorption spectrum (Figure 4a). As Cd is incorporated, both absorption shoulders redshift and become less distinct. This shift is accompanied by the corresponding PL redshift.

DOI: 10.1021/acs.chemmater.9b02615
Chem. Mater. 2019, 31, 9307−9316

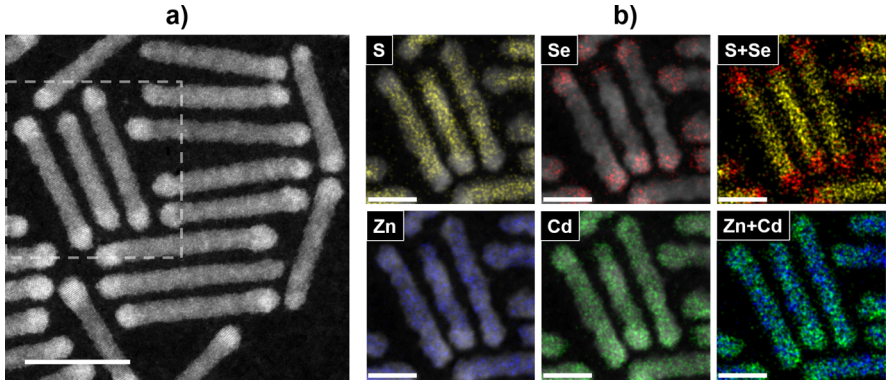

Figure 3. (a) HAADF-STEM image of HNRs exchanged with 0.25 mmol $CdCl_2$ and 1 mmol $ZnCl_2$. The scale bar is 20 nm. (b) EDS maps of the dashed region in (a). Individual atomic signals are overlaid on the HAADF intensity, and the sum of anion and cation signals are shown to their right. The scale bar is 10 nm.

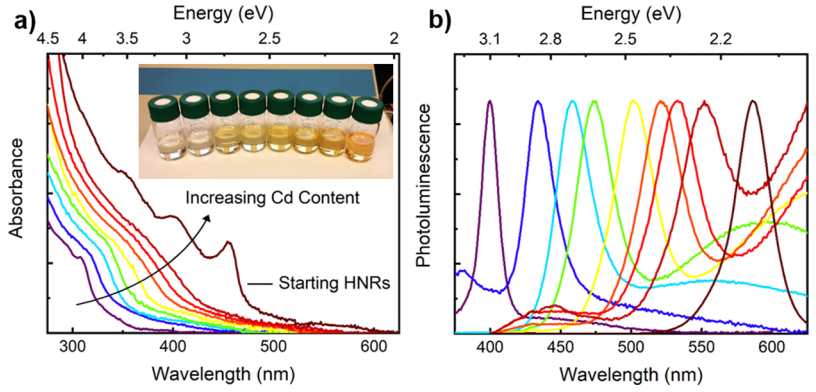

Figure 4. Absorption (a) and PL (b) spectra of HNRs after optimized Cd/Zn cation exchange including 1-octanethiol. Starting from the highest energy, 0, 0.02, 0.05, 0.1, 0.2, 0.3, 0.4, and 0.5 mmol $CdCl_2$ were mixed with 1 mmol $ZnCl_2$. A photo of the resulting solutions is shown as the inset of (a). The lowest energy spectrum corresponds to the starting CdS/CdSe HNRs. Almost the entire visible spectrum can be sampled by choosing the appropriate amount of Cd to be included.

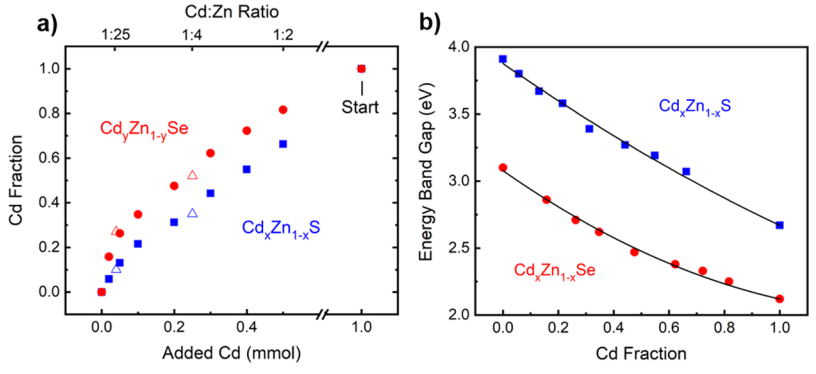

Figure 5. (a) HNR composition as a function of the amount of added Cd. Solid symbols were estimated by Vegard's Law, using measured lattice parameters from TEM. Open triangles indicate Cd fractions from EDS measurements. (b) Relationship between optical band gap and composition. The black lines are parabolic fits of the data, with bowing parameters equal to 0.24 eV for $Cd_xZn_{1-x}S$ and 0.49 eV for $Cd_ySe_{1-y}Se$.

There is also a broadening of the band edge PL from ~110 meV at the pure Cd and Zn conditions to ~175 meV when alloyed. The broad emission associated with thiol ligands that increases in intensity with increasing Cd content is also present and is discussed later. Nevertheless, band edge emission spanning the entire spectral range from pure ZnSe at 400 nm to the emission of CdSe around 600 nm can be achieved.

Figure 5a shows how the composition of the resulting HNRs varies with the ratio of Cd and Zn reagents added to the cation exchange reaction mixture. The composition is estimated by Vegard's Law using lattice parameters directly measured from high-resolution TEM images (Supporting Information Figure S9), taking the lattice spacing of CdS/CdSe HNRs and Zn-only cation exchange HNRs as the limits. The $Cd_xZn_{1-x}S$ component shows consistently less Cd incorporation than $Cd_ySe_{1-y}Se$, which is supported by the EDS results discussed earlier. Figure 5b shows the relation between the measured band gap of each component and the composition assigned by the lattice parameter. Here, the energy band gaps are estimated from the PL peak position for the selenide component and

DOI: 10.1021/acs.chemmater.9b02615
Chem. Mater. 2019, 31, 9307−9316

from the minimum of the first derivative of the absorption spectrum for the sulfide component. There is a slight deviation from linear dependence of the band gap on composition especially for the selenide component. Assuming similar degrees of quantum confinement regardless of alloying composition, this trend can be attributed to optical bowing. The solid lines in Figure 5b are fits to a parabolic function, leading to bowing parameters of 0.49 and 0.24 eV for Cd/Zn selenide and sulfide, respectively. These values agree well with literature reports.[37−40] Even including the optical bowing effect, three independent measurements of lattice spacing, EDS, and optical band gap indicate that the tips tend to end up with a higher Cd content than the centers of the rods.

We believe the difference in Cd incorporation between the different components can be attributed to the solubility product constant K_{sp} of each material. K_{sp} here describes the equilibrium configuration of the solid ionic compound versus its dissociation into suspended ions in the solvent.[21,41] A compound with a lower K_{sp} can spontaneously displace a compound of higher K_{sp} and initiate a cation exchange reaction (e.g., Cd^{2+} being displaced by Cu^{+}). Miszta et al. studied cation exchange of $Cu_{2-x}Se/Cu_{2-x}S$ core/shell NRs and observed preferential exchange of the core to Ag_2Se or HgSe while the shell remained $Cu_{2-x}S$.[41] They rationalized that cation exchange is thermodynamically driven and thus the guest cations specifically targeted the selenide core due to the higher stability of that compound compared to the sulfide. Because of the high concentration of vacancies in Cu_{2-x} chalcogenides, guest cations can sample the entire rod rather than being limited to a surface reaction.

Although in our case cation exchange occurs in a complex mixture of ligands and at elevated temperature, the underlying differences in K_{sp} may still be responsible for the observed inhomogeneity of the Cd distribution. Reported K_{sp} values for ZnS, ZnSe, CdS, and CdSe are 1.6×10^{-24}, 3.6×10^{-26}, 8×10^{-27}, and 4×10^{-35}, respectively.[21] In both sulfides and selenides, the Cd compound is less soluble and thus can outcompete Zn during cation exchange, which is why the actual Cd incorporation is always greater than the proportion of ions in solution. Furthermore, the difference in solubility between ZnSe and CdSe is far greater than that between ZnS and CdS, which explains why the selenide tips tend to accumulate more Cd and the rod centers are relatively Cd-deficient. To support this idea, we performed cation exchange reactions of single-component CdS NRs and CdSe NRs first to Cu and then to Cd/Zn under the same 1:4 Cd/Zn condition (Supporting Information Figure S10). The resulting NRs did not appear to have Cd-rich tips, and their compositions were the same as we observed in Figure 3. Starting with CdSe NRs led to more Cd incorporation throughout than starting with CdS NRs despite the identical reaction conditions. Therefore, the discrepancy in alloying composition does not appear to be due to local shape (e.g., curvature at the tips) or facet selectivity but rather the relative solubility of the target compounds. Because of these reasons, equal alloying from the rod center to tips may be difficult to achieve. Nevertheless, the fact that the sulfide component is more Zn-rich ensures that the conduction band edge remains slightly higher than that of the selenide, maintaining the desired (slight) type-I band offset that promotes radiative recombination at the tips.

We note that during the cation exchange reaction, a rapid color change from dark brown to yellow/orange (depending on the amount of Cd present) is observed without measurable band edge PL at short periods of time. However, stirring for 15 min or more gives rise to band edge emission from the rods. We believe that this appearance of the band edge PL results from the removal of remaining Cu impurities in the lattice, which have been shown to quench emission even when only one or two atoms are present within a NC.[42] Indeed, PL quenching from Cu incorporation can readily be seen during the initial Cu cation exchange step, when the addition of only 50 μL of the Cu source strongly quenches the emission. Our result is similar to that of Jain et al., who showed that mild annealing in the presence of phosphine could purify NCs of this residual Cu and restore their PL.[42] Therefore, we stirred the cation exchange solutions for 1 h after HNR injection. However, broad red emission could be observed as well, especially for samples with larger degrees of Cd incorporation (Figure 4b). We suspect that the presence of thiols, which are known hole traps for CdSe,[43,44] are causing this emission.

As a control experiment to verify thiol-induced deep trap emission and recovery of the original CdS/CdSe composition, HNRs were exchanged back to Cd after the intermediate Cu cation exchange step. The same method using thiols was carried out for the second cation exchange step with $CdCl_2$ completely replacing $ZnCl_2$. In this case, the broad emission dominates, and the band edge PL was only 1/10 as intense as the starting HNRs (Supporting Information Figure S11). If no thiols were used, the band edge PL was comparable to the starting HNRs and only a small amount of broad red emission was observed. The absorption spectrum redshifted slightly but maintained all the same features. This slight red-shift is likely due to the surface adsorbed Cd. As synthesized, the barbell-shaped HNR surface is terminated largely with Zn-OA,[13] but after cation exchange, the surface is terminated with Cd, leading effectively to a slightly larger diameter and therefore a smaller degree of carrier confinement.

While this broad red emission appears to be from thiol traps, it also resembles Cu dopant emission.[45,46] Considering that the band edge PL continues to improve over time post-cation exchange, it is likely that there is some small amount of retained Cu, even after 1 h. We performed inductively coupled plasma mass spectrometry (ICP-MS) on our cation-exchanged HNRs and measured a Cu cation composition of 0.132 ± 0.0064% (i.e., [Cu]/([Cd] + [Zn] + [Cu]). While this Cu concentration is too low to cause changes in the absorption spectra, even a small number of Cu atoms can act as color centers for PL. Therefore, we carried out time-resolved PL measurements on our cation-exchanged HNRs. For comparison, we also measured CdS/CdSe HNRs that showed trap emission. The static PL spectra and the time-resolved PL data are available in Figure S12. The broad red emission in cation-exchanged HNRs includes a long-lived component with a time constant >1300 ns, which is much longer than band edge emission or "native" deep-trap emission, suggesting that the broad emission is due to Cu dopants rather than thiol-induced traps.[46,47] We note that the long-lived component in cation-exchanged HNRs are only prominent in the presence of octanethiol, indicating that thiols may act as a mediator to transfer trapped charges to the dopant color centers.[48]

At first glance their undesirable contribution to PL characteristics might be detrimental to developing highly luminescent DHNRs because thiols are integral to achieving controlled degrees of Cd incorporation under the conditions explored here. However, an additional shell layer (e.g., partial ZnSe to achieve DHNR structure) can be grown on the

DOI: 10.1021/acs.chemmater.9b02615
Chem. Mater. 2019, 31, 9307−9316

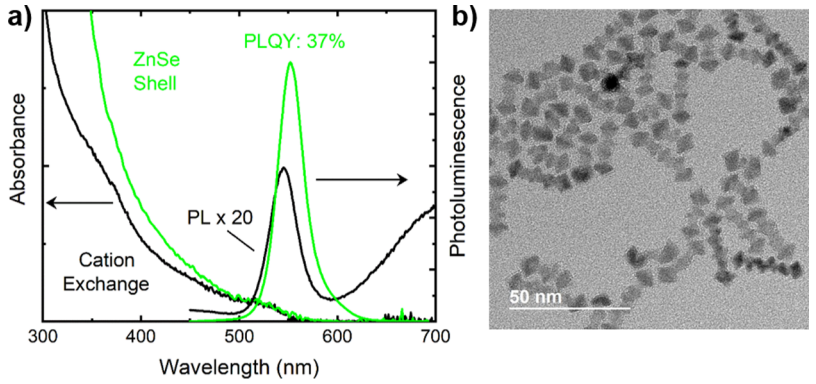

Figure 6. ZnSe shell growth on cation-exchanged HNRs. (a) Absorption and PL spectra of green DHNRs. The HNRs were exchanged using 0.3 mmol $CdCl_2$. (b) Low-resolution TEM showing the structure of green DHNRs after shell growth.

achieved $Cd_xZn_{1-x}S/Cd_yZn_{1-y}Se$ alloyed HNRs to alleviate this problem as discussed in the next section.

ZnSe Growth for the DHNR Structure. Although the band-edge emission color can be well-tuned by the above two-step cation exchange approach to HNRs, the PL is relatively low and often includes broad dopant emission. To improve PL and to achieve the desired double heterostructure band alignment, a ZnSe shell, mostly on the selenide tips initially, was grown by injecting cation-exchanged and cleaned HNRs into a Zn-OA solution with TOP−Se at high temperature. An example of the resulting absorption and PL spectra after ZnSe growth is shown in Figure 6a, with a representative TEM image in Figure 6b. For this particular case, the HNRs had been exchanged using 0.3 mmol $CdCl_2$ and 1.0 mmol $ZnCl_2$ prior to ZnSe growth to yield green emission. ZnSe growth leads to an increase in absorption above 400 nm and a large ∼30× increase in PL, leading to PL QY of 37% for excitation at 443 nm and no observable trap emission at room temperature. The rods themselves show significant growths both at the tips and sides with very little redshift in the PL, indicating a relatively large amount of ZnSe shell has grown without the ripening of the emitting Cd/Zn selenide tips. Further optimization of this ZnSe growth step may lead to even higher PL QYs.

To gain further insights on cation exchange vs. surface adsorption effects on PL, red-emitting DHNRs synthesized through the two cation exchange steps were also compared to similar wavelength emitting DHNRs synthesized directly without cation exchange step. One batch of CdS/CdSe HNRs was split into three parts. For the first part, a ZnSe shell was grown directly following the established method to form DHNRs (referred to here as "regular" DHNRs).[10] The second part was exchanged with Cu, back exchanged to pure Cd using 1 mmol $CdCl_2$ with no Zn and then further grown with a ZnSe shell to form DHNRs ("cation exchanged"). The final third was injected into the $CdCl_2$/oleylamine solution to mimic the surface of cation-exchanged HNRs without Cu intermediate exchange before ZnSe shell growth ("$CdCl_2$ treated"). The resulting absorption and PL spectra are shown in Figure 7. Representative TEM images are available in Supporting Information Figure S13. The CdS/CdSe absorption spectra of the three samples just prior to ZnSe growth (dotted lines) appear nearly identical. After the shell growth, a large increase in the absorption above 400 nm indicative of ZnSe growth is observed. For the samples with a Cd-rich surface ($CdCl_2$ treated and cation exchanged), a significant

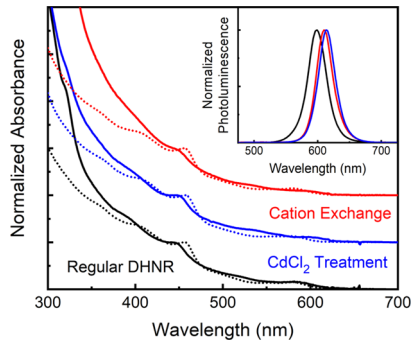

Figure 7. Absorption and PL (inset) spectra of CdS/CdSe HNRs (dotted lines) and DHNRs (solid lines) comparing the effects of cation exchange steps and exposure to $CdCl_2$. The spectra are normalized for comparison. Samples with a Cd-rich surface (cation exchange and $CdCl_2$ treatment) show a noticeable redshift after shell growth.

redshift in both the absorption and PL spectra is seen after the shell growth. Presumably, the surface-adsorbed Cd gets consumed to grow CdSe before any ZnSe is grown. The cation-exchanged DHNRs maintain comparable PL QY of the band edge emission compared to regular DHNRs, indicating that no irreparable damage has been rendered by the cation exchange process.

PL spectra from a series of DHNRs that exhibit red, green, and blue emission achieved through our cation exchange approach are shown in Figure 8. In each case, narrow (≤31 nm) linewidths are obtained. RGB DHNRs synthesized by cation exchange show similar PL decay properties to standard DHNRs[49] (Supporting Information Figure S14), indicating that the unique band offsets are preserved after cation exchange. PL QY for blue emission is ∼10%. To achieve emission this blue, the HNRs were exchanged with a 1:25 ratio of Cd/Zn. The tips are close in composition to ZnSe and thus a ZnSe shell may not adequately protect them. Our best results for green DHNRs, on the other hand, showed similar PL QY to the red control experiment (37 and 44%, respectively). It may be possible to enhance the emission even further, especially for blue DHNRs, by growing a ZnS or ZnS_xSe_{1-x} outer shell, but we leave this optimization for future investigations. Here, we have achieved respectable PL across the entire visible spectrum without the use of a ZnS outer shell, maintaining a double-heterojunction energy level alignment with an anisotropic shape that can efficiently guide electrons and holes to the $Cd_xZn_{1-x}Se$ emitter.

DOI: 10.1021/acs.chemmater.9b02615
Chem. Mater. 2019, 31, 9307−9316

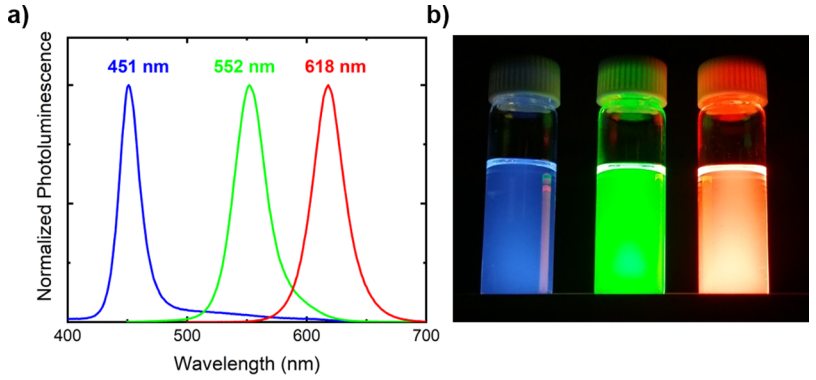

Figure 8. (a) PL spectra of a series red, green, and blue-emitting DHNRs achieved through two-step cation exchange. (b) Photograph of DHNR solutions under UV excitation.

CONCLUSIONS

In conclusion, we have demonstrated the synthesis of a series of DHNRs with emission covering nearly the entire visible spectrum through cation exchange-induced alloying. By employing Cu-OA and oleylamine, we minimized NR aggregation and reaction yield loss from the first Cu exchange step. Using a mixture of $CdCl_2$ and $ZnCl_2$ in the presence of 1-octanethiol, we achieved controllable amounts of Cd incorporation in both components. The low efficiency postcation exchange PL could be substantially improved by subsequent growth of a ZnSe shell, leading to narrow, single-peak emission. This degree of control over the band gap and emission color combined with the double heterostructure band alignment is ideally suited for integration into optoelectronic devices. The methods detailed here lay the groundwork for controllable Cd/Zn alloying of sulfides and selenides (and possibly even tellurides) of anisotropic NC heterostructures, which can be first grown to the desired shape and size through well-developed synthesis methods and alloyed afterward under mild conditions to the desired band gap.

EXPERIMENTAL SECTION

Synthesis. Detailed description of the synthesis is given in the Supporting Information. Cu cation exchange was carried out exclusively in a N_2-filled glove box. Cation exchange using tetrakis(acetonitrile)copper(I) hexafluorophosphate ($[Cu(CH_3CN)_4]PF_6$) followed a literature method with some modifications.[20] TOPO (0.2 g) was first added to a cleaned NR or HNR solution. Then, 0.05 M $[Cu(CH_3CN)_4]PF_6$ solution in anhydrous methanol was added incrementally (up to 2 mL as indicated), stirring for 2 min between additions, including the final addition. The NRs were precipitated by centrifugation, and the resulting pellet was rinsed with anhydrous methanol. Then, it was dissolved in 2 mL TOP by sonication for the Zn/Cd exchange step.

For cation exchange using Cu(I)-oleate (Cu-OA), 100 μL of oleylamine was first added to a cleaned NR or HNR solution. Then, 0.1 M Cu-OA solution [separately prepared by dissolving and degassing 2 mmol of Cu(I) acetate and 16 mmol oleic acid (OA) in 14.8 mL octadecene (ODE)] was added incrementally in the same manner as the $[Cu(CH_3CN)_4]PF_6$ case. The product was purified as detailed above after adding 5 mL of anhydrous methanol to induce flocculation.

Zn cation exchange was performed by modifying procedures given by ref 20. A mixture of 1 mmol $ZnCl_2$, 2 mL oleylamine, and 3 mL ODE was degassed for 1 h at 110 °C under vigorous stirring and heated to 170 °C for 20 min under an Ar flow. Half of the product from the Cu-exchange step dissolved in TOP was injected at 150 °C. The reaction mixture was stirred for 1 h and then cooled to room temperature. Zn/Cd cation exchange was performed in a similar manner by adding specified amounts of $CdCl_2$ to the initial reaction mixture and then injecting Cu-exchanged NRs or HNRs with 0.5 mL 1-octanethiol.

ZnSe was grown over the cation-exchanged HNRs, following a similar procedure reported previously.[13] First, 0.5 mmol Zn acetate, 6 mmol OA, and 1.1 mL ODE were degassed for 30 min at 110 °C and heated to 310 °C. Then, a solution of cleaned HNRs, 0.15 mL of 1 M TOP−Se and 0.45 mL of TOP were injected into the reaction mixture and allowed to stir for 30 s before being quenched by air jet. The standard shell growth procedure used for red DHNRs employs a 1:4 molar ratio of Zn/OA and growth for 2 min.[10]

Characterization. STEM and TEM samples were prepared by drop-casting a solution of HNRs in chloroform onto a Cu grid with ultrathin carbon film (electron microscopy sciences). Analysis was carried out on a JEOL 2100 TEM operating at 200 kV. High-angle annular dark field (HAADF) STEM and energy-dispersive EDS was performed on an FEI THEMIS Z aberration corrected TEM/STEM operating at 300 kV. XRD samples were prepared by drop-casting HNR solutions in chloroform onto a 1 cm^2 glass slide. Powder XRD was obtained using a Rigaku Miniflex 600. Simulated diffraction patterns were generated using CrystalMaker 9. HNR solutions were prepared for ICP-MS analysis by three additional precipitation/redissolution cycles in methanol/chloroform. Aqua regia was made by combining fuming HCl and fuming HNO_3 in a 3:1 ratio to a total volume of 4 mL, and this solution was used to digest the HNRs.[50] A portion of the digested solution was then transferred to a volumetric flask and diluted by the addition of deionized water. Elements Cd and Zn were analyzed using an Optima 8300 ICP-OES, and Cu was analyzed using a NexION 350D. Five samples at different dilutions were examined. UV−vis absorption spectra were collected with an Agilent 8453 photodiode array spectrometer. Near-infrared (NIR) absorption spectra were collected with a Varian Cary5G spectrometer. PL spectra were collected with a HORIBA Jobin Yvon FluoroMax-3 fluorometer. PL QY for red and green DHNRs was measured against a DCM reference at 443 nm and confirmed by measuring absolute PL QY using a HORIBA Jobin Yvon Nanolog fluorometer equipped with an integrating sphere. PL QY for blue DHNRs was measured with excitation wavelength of 380 nm. PL lifetime measurements were performed by time-correlated single photon counting, with a 400 nm Delta Diode laser serving as the excitation.

ASSOCIATED CONTENT

Supporting Information

The Supporting Information is available free of charge on the ACS Publications website at DOI: 10.1021/acs.chemmater.9b02615.

More detailed synthesis procedures and results from sub-optimal cation exchange procedures, control experiments, and additional TEM (PDF)

DOI: 10.1021/acs.chemmater.9b02615
Chem. Mater. 2019, 31, 9307−9316

AUTHOR INFORMATION

Corresponding Author

*E-mail: mshim@illinois.edu.

ORCID

Joseph C. Flanagan: 0000-0002-4090-4149
Logan P. Keating: 0000-0002-1106-9658
Muttanagoud N. Kalasad: 0000-0002-6006-0174
Moonsub Shim: 0000-0001-7781-1029

Present Address

[†]Department of Physics, Davangere University, Davangere, India.

Notes

The authors declare no competing financial interest.

ACKNOWLEDGMENTS

This material is based upon work supported by the National Science Foundation (grant no. 1808163). TEM, STEM, and NIR absorption measurements were carried out in the Frederick Seitz Materials Research Laboratory Central Research Facilities, University of Illinois. We thank Dr. James Mabon for help collecting the EDS maps. ICP-MS was carried out in the Microanalysis Laboratory of the University of Illinois at Urbana Champaign. We thank Dr. Kiran Subedi for his assistance in the elemental analysis.

REFERENCES

(1) Ma, F.; Li, C.-C.; Zhang, C.-Y. Development of Quantum Dot-Based Biosensors: Principles and Applications. *J. Mater. Chem. B* **2018**, *6*, 6173−6190.

(2) Jiang, Y.; Cho, S.-Y.; Shim, M. Light-Emitting Diodes of Colloidal Quantum Dots and Nanorod Heterostructures for Future Emissive Displays. *J. Mater. Chem. C* **2018**, *6*, 2618−2634.

(3) Choi, M. K.; Yang, J.; Hyeon, T.; Kim, D.-H. Flexible Quantum Dot Light-Emitting Diodes for Next-Generation Displays. *npj Flexible Electron.* **2018**, *2*, 10.

(4) Meinardi, F.; Bruni, F.; Brovelli, S. Luminescent Solar Concentrators for Building-Integrated Photovoltaics. *Nat. Rev. Mater.* **2017**, *2*, 17072.

(5) Hines, D. A.; Kamat, P. V. Recent Advances in Quantum Dot Surface Chemistry. *ACS Appl. Mater. Interfaces* **2014**, *6*, 3041−3057.

(6) Carey, G. H.; Abdelhady, A. L.; Ning, Z.; Thon, S. M.; Bakr, O. M.; Sargent, E. H. Colloidal Quantum Dot Solar Cells. *Chem. Rev.* **2015**, *115*, 12732−12763.

(7) Pan, Z.; Rao, H.; Mora-Seró, I.; Bisquert, J.; Zhong, X. Quantum Dot-Sensitized Solar Cells. *Chem. Soc. Rev.* **2018**, *47*, 7659−7702.

(8) Scarfiello, R.; Nobile, C.; Cozzoli, P. D. Colloidal Magnetic Heterostructured Nanocrystals with Asymmetric Topologies: Seeded-Growth Synthetic Routes and Formation Mechanisms. *Front. Mater.* **2016**, *3*, 56.

(9) Lv, H.; Wang, C.; Li, G.; Burke, R.; Krauss, T. D.; Gao, Y.; Eisenberg, R. Semiconductor Quantum Dot-Sensitized Rainbow Photocathode for Effective Photoelectrochemical Hydrogen Generation. *Proc. Natl. Acad. Sci. U.S.A.* **2017**, *114*, 11297−11302.

(10) Oh, N.; Nam, S.; Zhai, Y.; Deshpande, K.; Trefonas, P.; Shim, M. Double-Heterojunction Nanorods. *Nat. Commun.* **2014**, *5*, 3642.

(11) Nam, S.; Oh, N.; Zhai, Y.; Shim, M. High Efficiency and Optical Anisotropy in Double-Heterojunction Nanorod Light-Emitting Diodes. *ACS Nano* **2015**, *9*, 878−885.

(12) Oh, N.; Kim, B. H.; Cho, S.-Y.; Nam, S.; Rogers, S. P.; Jiang, Y.; Flanagan, J. C.; Zhai, Y.; Kim, J.-H.; Lee, J.; Yu, Y.; Cho, Y. K.; Hur, G.; Zhang, J.; Trefonas, P.; Rogers, J. A.; Shim, M. Double-Heterojunction Light-Responsive LEDs for Display Applications. *Science* **2017**, *355*, 616−619.

(13) Oh, N.; Shim, M. Metal Oleate Induced Etching and Growth of Semiconductor Nanocrystals, Nanorods, and Their Heterostructures. *J. Am. Chem. Soc.* **2016**, *138*, 10444−10451.

(14) Jia, G.; Banin, U. A General Strategy for Synthesizing Colloidal Semiconductor Zinc Chalcogenide Quantum Rods. *J. Am. Chem. Soc.* **2014**, *136*, 11121−11127.

(15) Kumar, V.; Fustér, H. A.; Oh, N.; Zhai, Y.; Deshpande, K.; Shim, M.; Kenis, P. J. A. Continuous Flow Synthesis of Anisotropic Cadmium Selenide and Zinc Selenide Nanoparticles. *ChemNanoMat* **2017**, *3*, 204−211.

(16) Zhong, X.; Feng, Y.; Zhang, Y.; Gu, Z.; Zou, L. A Facile Route to Violet- to Orange-Emitting $Cd_xZn_{1-x}Se$ Alloy Nanocrystals via Cation Exchange Reaction. *Nanotechnology* **2007**, *18*, 385606.

(17) Groeneveld, E.; Witteman, L.; Lefferts, M.; Ke, X.; Bals, S.; Van Tendeloo, G.; de Mello Donega, C. Tailoring ZnSe-CdSe Colloidal Quantum Dots via Cation Exchange: From Core/Shell to Alloy Nanocrystals. *ACS Nano* **2013**, *7*, 7913−7930.

(18) Choi, J. Y.; Nam, K. M.; Song, H. Composition Effect of Alloy Semiconductors on Pt-tipped $Zn_{1-x}Cd_xSe$ Nanorods for Enhanced Photocatalytic Hydrogen Generation. *J. Mater. Chem. A* **2018**, *6*, 16316−16321.

(19) Li, H.; Zanella, M.; Genovese, A.; Povia, M.; Falqui, A.; Giannini, C.; Manna, L. Sequential Cation Exchange in Nanocrystals: Preservation of Crystal Phase and Formation of Metastable Phases. *Nano Lett.* **2011**, *11*, 4964−4970.

(20) Li, H.; Brescia, R.; Krahne, R.; Bertoni, G.; Alcocer, M. J. P.; D'Andrea, C.; Scotognella, F.; Tassone, F.; Zanella, M.; De Giorgi, M.; Manna, L. Blue-UV-Emitting ZnSe(Dot)ZnS(Rod) Core/Shell Nanocrystals Prepared from CdSe/CdS Nanocrystals by Sequential Cation Exchange. *ACS Nano* **2012**, *6*, 1637−1647.

(21) De Trizio, L.; Manna, L. Forging Colloidal Nanostructures via Cation Exchange Reactions. *Chem. Rev.* **2016**, *116*, 10852−10887.

(22) Liu, Y.; Liu, M.; Yin, D.; Qiao, L.; Fu, Z.; Swihart, M. T. Selective Cation Incorporation into Copper Sulfide Based Nanoheterostructures. *ACS Nano* **2018**, *12*, 7803−7811.

(23) Liu, Y.; Yin, D.; Swihart, M. T. Valence Selectivity of Cation Incorporation into Covellite CuS Nanoplatelets. *Chem. Mater.* **2018**, *30*, 1399−1407.

(24) Fenton, J. L.; Steimle, B. C.; Schaak, R. E. Tunable Intraparticle Frameworks for Creating Complex Heterostructured Nanoparticle Libraries. *Science* **2018**, *360*, 513−517.

(25) Yuan, Y.; Zhu, H.; Wang, X.; Cui, D.; Gao, Z.; Su, D.; Zhao, J.; Chen, O. Cu-Catalyzed Synthesis of CdZnSe−CdZnS Alloy Quantum Dots with Highly Tunable Emission. *Chem. Mater.* **2019**, *31*, 2636−2643.

(26) Zhang, Y. C.; Chen, W. W.; Hu, X. Y. Controllable Synthesis and Optical Properties of Zn-Doped CdS Nanorods from Single-Source Molecular Precursors. *Cryst. Growth Des.* **2007**, *7*, 580−586.

(27) Zhang, Y.; Cai, J.; Ji, T.; Wu, Q.; Xu, Y.; Wang, X.; Sun, T.; Yang, L.; Hu, Z. Superionic Conductor-Mediated Growth of Ternary ZnCdS Nanorods over a Wide Composition Range. *Nano Res.* **2015**, *8*, 584−591.

(28) Ma, A.; Tang, Z.; Shen, S.; Zhi, L.; Yang, J. Controlled Synthesis of $Zn_xCd_{1-x}S$ Nanorods and their Composite with RGO for High-Performance Visible-Light Photocatalysis. *RSC Adv.* **2015**, *5*, 27829−27836.

(29) Sadtler, B.; Demchenko, D. O.; Zheng, H.; Hughes, S. M.; Merkle, M. G.; Dahmen, U.; Wang, L.-W.; Alivisatos, A. P. Selective Facet Reactivity during Cation Exchange in Cadmium Sulfide Nanorods. *J. Am. Chem. Soc.* **2009**, *131*, 5285−5293.

(30) Kriegel, I.; Wisnet, A.; Kandada, A. R. S.; Scotognella, F.; Tassone, F.; Scheu, C.; Zhang, H.; Govorov, A. O.; Rodríguez-Fernández, J.; Feldmann, J. Cation Exchange Synthesis and Optoelectronic Properties of Type II CdTe−$Cu_{2-x}Te$ Nano-Heterostructures. *J. Mater. Chem. C* **2014**, *2*, 3189−3198.

(31) Houck, D. W.; Assaf, E. I.; Shin, H.; Greene, R. M.; Pernik, D. R.; Korgel, B. A. Pervasive Cation Vacancies and Antisite Defects in Copper Indium Diselenide ($CuInSe_2$) Nanocrystals. *J. Phys. Chem. C* **2019**, *123*, 9544−9551.

DOI: 10.1021/acs.chemmater.9b02615
Chem. Mater. 2019, 31, 9307−9316

(32) Lesnyak, V.; Brescia, R.; Messina, G. C.; Manna, L. Cu Vacancies Boost Cation Exchange Reactions in Copper Selenide Nanocrystals. *J. Am. Chem. Soc.* **2015**, *137*, 9315−9323.
(33) Luther, J. M.; Zheng, H.; Sadtler, B.; Alivisatos, A. P. Synthesis of PbS Nanorods and Other Ionic Nanocrystals of Complex Morphology by Sequential Cation Exchange Reactions. *J. Am. Chem. Soc.* **2009**, *131*, 16851−16857.
(34) Hamer, D. H. Metallothionein. *Annu. Rev. Biochem.* **1986**, *55*, 913−951.
(35) Walsh, M. J.; Ahner, B. A. Determination of Stability Constants of Cu(I), Cd(II) & Zn(II) Complexes with Thiols using Fluorescent Probes. *J. Inorg. Biochem.* **2013**, *128*, 112−123.
(36) Pearson, R. G. Hard and Soft Acids and Bases. *J. Am. Chem. Soc.* **1963**, *85*, 3533−3539.
(37) Venugopal, R.; Lin, P.-I.; Chen, Y.-T. Photoluminescence and Raman Scattering from Catalytically Grown $Zn_xCd_{1-x}Se$ Alloy Nanowires. *J. Phys. Chem. B* **2006**, *110*, 11691−11696.
(38) Mourad, D.; Czycholl, G.; Kruse, C.; Klembt, S.; Retzlaff, R.; Hommel, D.; Gartner, M.; Anastasescu, M. Band Gap Bowing of Binary Alloys: Experimental Results Compared to Theoretical Tight-Binding Supercell Calculations for $Cd_xZn_{1-x}Se$. *Phys. Rev. B: Condens. Matter Mater. Phys.* **2010**, *82*, 165204.
(39) Zhong, X.; Feng, Y.; Knoll, W.; Han, M. Alloyed $Zn_xCd_{1-x}S$ Nanocrystals with Highly Narrow Luminescence Spectral Width. *J. Am. Chem. Soc.* **2003**, *125*, 13559−13563.
(40) Li, M.; Jiang, J.; Guo, L. Characterization, and Photoelectrochemical Study of $Cd_{1-x}Zn_xS$ Solid Solution Thin Films Deposited by Spray Pyrolysis for Water Splitting. *Int. J. Hydrogen Energy* **2010**, *35*, 7036−7042.
(41) Miszta, K.; Gariano, G.; Brescia, R.; Marras, S.; De Donato, F.; Ghosh, S.; De Trizio, L.; Manna, L. Selective Cation Exchange in the Core Region of $Cu_{2-x}Se/Cu_{2-x}S$ Core/Shell Nanocrystals. *J. Am. Chem. Soc.* **2015**, *137*, 12195−12198.
(42) Jain, P. K.; Beberwyck, B. J.; Fong, L.-K.; Polking, M. J.; Alivisatos, A. P. Highly Luminescent Nanocrystals From Removal of Impurity Atoms Residual From Ion-Exchange Synthesis. *Angew. Chem.* **2012**, *51*, 2387−2390.
(43) Wuister, S. F.; de Mello Donegá, C.; Meijerink, A. Influence of Thiol Capping on the Exciton Luminescence and Decay Kinetics of CdTe and CdSe Quantum Dots. *J. Phys. Chem. B* **2004**, *108*, 17393−17397.
(44) Baker, D. R.; Kamat, P. V. Tuning the Emission of CdSe Quantum Dots by Controlled Trap Enhancement. *Langmuir* **2010**, *26*, 11272−11276.
(45) Pradhan, N.; Goorskey, D.; Thessing, J.; Peng, X. An Alternative of CdSe Nanocrystal Emitters: Pure and Tunable Impurity Emissions in ZnSe Nanocrystals. *J. Am. Chem. Soc.* **2005**, *127*, 17586−17587.
(46) Srivastava, B. B.; Jana, S.; Pradhan, N. Doping Cu in Semiconductor Nanocrystals: Some Old and Some New Physical Insights. *J. Am. Chem. Soc.* **2011**, *133*, 1007−1015.
(47) Gul, S.; Cooper, J. K.; Corrado, C.; Vollbrecht, B.; Bridges, F.; Guo, J.; Zhang, J. Z. Synthesis, Optical and Structural Properties, and Charge Carrier Dynamics of Cu-Doped ZnSe Nanocrystals. *J. Phys. Chem. C* **2011**, *115*, 20864−20875.
(48) Maiti, S.; Chen, H.-Y.; Park, Y.; Son, D. H. Evidence for the Ligand-Assisted Energy Transfer from Trapped Exciton to Dopant in Mn-Doped CdS/ZnS Semiconductor Nanocrystals. *J. Phys. Chem. C* **2014**, *118*, 18226−18232.
(49) Drake, G. A.; Flanagan, J. C.; Shim, M. Highly Luminescent Double-Heterojunction Nanorods. *J. Chem. Phys.* **2019**, *151*, 134706.
(50) Yu, W. W.; Qu, L.; Guo, W.; Peng, X. Experimental Determination of the Extinction Coefficient of CdTe, CdSe, and CdS Nanocrystals. *Chem. Mater.* **2003**, *15*, 2854−2860.

DOI: 10.1021/acs.chemmater.9b02615
Chem. Mater. 2019, 31, 9307−9316